

## Patterning via surface monolayer initiated polymerization: A study of surface initiator photoreaction kinetics

Kendra McCoy, Dennis W. Hess, Clifford L. Henderson, and Laren M. Tolbert

Citation: *J. Vac. Sci. Technol. B* **22**, 3503 (2004); doi: 10.1116/1.1824061

View online: <http://dx.doi.org/10.1116/1.1824061>

View Table of Contents: <http://avspublications.org/resource/1/JVTBD9/v22/i6>

Published by the AVS: Science & Technology of Materials, Interfaces, and Processing

---

### Additional information on J. Vac. Sci. Technol. B

Journal Homepage: <http://avspublications.org/jvstb>

Journal Information: [http://avspublications.org/jvstb/about/about\\_the\\_journal](http://avspublications.org/jvstb/about/about_the_journal)


Top downloads: [http://avspublications.org/jvstb/top\\_20\\_most\\_downloaded](http://avspublications.org/jvstb/top_20_most_downloaded)

Information for Authors: [http://avspublications.org/jvstb/authors/information\\_for\\_contributors](http://avspublications.org/jvstb/authors/information_for_contributors)

## ADVERTISEMENT


# Instruments for advanced science

**Gas Analysis**




- dynamic measurement of reaction gas streams
- catalysis and thermal analysis
- molecular beam studies
- dissolved species probes
- fermentation, environmental and ecological studies

**Surface Science**




- UHV TPD
- SIMS
- end point detection in ion beam etch
- elemental imaging - surface mapping

**Plasma Diagnostics**



- plasma source characterization
- etch and deposition process reaction kinetic studies
- analysis of neutral and radical species

**Vacuum Analysis**



- partial pressure measurement and control of process gases
- reactive sputter process control
- vacuum diagnostics
- vacuum coating process monitoring

contact Hiden Analytical for further details

**HIDEN ANALYTICAL**

[info@hideninc.com](mailto:info@hideninc.com)  
[www.HidenAnalytical.com](http://www.HidenAnalytical.com)

CLICK to view our product catalogue 

# Patterning via surface monolayer initiated polymerization: A study of surface initiator photoreaction kinetics

Kendra McCoy, Dennis W. Hess, and Clifford L. Henderson<sup>a)</sup>  
*School of Chemical and Biomolecular Engineering, Georgia Institute of Technology,  
Atlanta, Georgia 30332-0100*

Laren M. Tolbert  
*School of Chemistry and Biochemistry, Georgia Institute of Technology, Atlanta, Georgia 30332*

(Received 4 June 2004; accepted 4 October 2004; published 14 December 2004)

Surface monolayer initiated polymerization (SMIP) is a potential method for achieving high resolution patterning of surfaces and materials that could be used as an alternative to conventional lithographic methods based on photoresist thin films. This article reports on the photochemical kinetic rate constants of two candidate azo-type surface bound photoradical initiator molecules. X-ray photoelectron spectroscopy was utilized to monitor the relative concentration of azo initiator on a silicon surface as a function of exposure dose to 248 nm radiation. This photochemical decomposition data showed that the photoreaction for both initiators followed first order kinetics with photoreaction rate constants in the range of  $4.5 \times 10^{-3} \text{ cm}^2/\text{mJ}$  to  $9.7 \times 10^{-3} \text{ cm}^2/\text{mJ}$ . The difference in the observed rate constants for the two azo initiators was attributed primarily to differences in their quantum efficiencies. These differences in quantum efficiency were attributed to the size of the nontethered fragment that would be produced from the initiator, with larger fragments producing slower photochemical decomposition kinetics. Thus, photoradical initiators with small non-surface bound fragments are desirable in terms of increasing the photosensitivity of such SMIP processes. For successful positive tone imaging using a SMIP process with photoradical initiators, it was estimated that approximately 99% of the monolayer must be decomposed in order to produce images in the resulting polymer layers. Using this information in conjunction with the photochemical reaction rate constants for the azo initiators, exposure doses on the order of  $400 \text{ mJ}/\text{cm}^2$  and larger would be required for the present initiators. © 2004 American Vacuum Society. [DOI: 10.1116/1.1824061]

## I. INTRODUCTION

Developing photoresists and processes for sub-100 nm lithography is a challenging and important task for both future semiconductor manufacturing as well as other emerging areas requiring nanopatterning. Conventional photoresists used for subtractive processing are typically comprised of organic polymers, and as the exposure wavelengths of optical lithography tools are decreased these materials often suffer from opacity problems.<sup>1</sup> In conventional single layer resist processing, this opacity problem can be solved in two ways: using thinner resist films or developing more transparent polymers. Both of these solutions are difficult to implement. Thinner resist layers present etch resistance limitations, while developing sufficiently transparent materials for low wavelength lithography has also proven to be difficult.<sup>2-4</sup> Top surface imaging (TSI), which can actually exploit the opacity of conventional resists, has previously been proposed as a solution to the problem. In TSI methods, a thin surface layer of the resist is exposed and used to create a pattern that can be transferred throughout the depth of the film. Conventional TSI approaches have primarily involved introducing silicon compounds into the surface of the film after ex-

posure and subsequently patterning the resist using dry etch methods.<sup>5,6</sup> These methods have been found to exhibit substantial line edge roughness and thus have not been widely adopted for use in advanced lithography.<sup>7</sup> The focus of this work has been to extend the idea of TSI to molecularly thin layers using an additive processing approach and solely organic materials. The method being investigated, called surface monolayer initiated polymerization (SMIP), involves patterning an initiator monolayer via radiation exposure and subsequently amplifying it by growing a polymer from that monolayer. Figure 1 shows a schematic of this process. In general, the approach taken in this work is similar in nature to the “grafting form” techniques originally reported by Ruehe and co-workers<sup>8,9</sup> and to the “cationic graft lithography” methods reported by Willson and co-workers.<sup>10,11</sup> This work on SMIP processes has focused in particular on the use of surface bound free radical initiators and the characterization of the photosensitivity of positive tone processes based on this design.

Processing films via this SMIP process offers an advantage as compared to other more complicated techniques in that it only requires as many steps as a conventional positive tone lithographic process. Instead of coating a resist film with a thickness on the order of several hundred nanometers, a thin self-assembled monolayer is first coated onto the substrate. This monolayer is composed of molecules that can

<sup>a)</sup>Author to whom correspondence should be addressed; electronic mail: cliff.henderson@chbe.gatech.edu

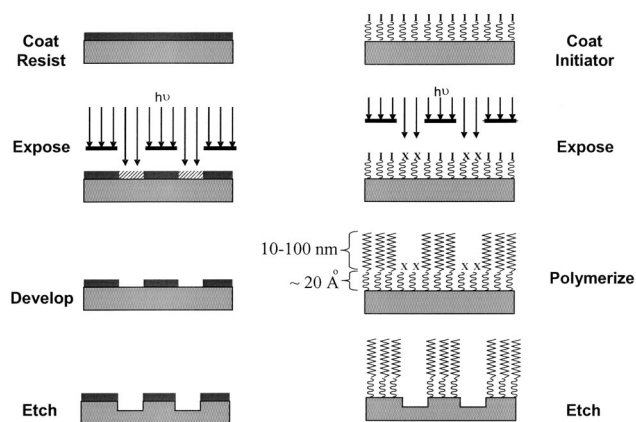


FIG. 1. Schematic of positive-tone SMIP process shown in comparison to positive tone conventional lithographic process.

subsequently be activated to initiate polymerization (i.e., the monolayer can form radical or ionic initiator species), and it is of the order of 1 nm thick. In the positive tone example shown in Fig. 1, this monolayer is then exposed to patterned radiation (e.g., ultraviolet light). The exposed regions of this monolayer react with the ambient and become deactivated. The substrate with the patterned monolayer is then placed in an environment with an appropriate monomer (e.g., a vinyl monomer for radical polymerization) and the remaining active monolayer regions are activated using either heat or radiation exposure to initiate polymerization. In this way, the original pattern formed in the monolayer is amplified into a thicker and more robust polymer pattern. There are no opacity issues when utilizing this process for sub-100 nm lithography since the original patterning is performed in a thin monolayer. The optical properties of the final polymer grown do not play a role in the exposure process. Therefore, the imaging characteristics of the process are completely controlled by the chemistry of the initiator, while the etch resistance of the resist pattern is completely controlled by the properties of the polymer formed during polymerization. Thus, using this approach it is possible to independently optimize the imaging and etch characteristics of the process. For example, for the same final resist thickness, significantly more etch resistant polymers can be used as etch masks via the SMIP process as compared to conventional single layer photoresists. This is because highly aromatic polymers that would be too absorbing for normal low wavelength lithographic processes can be used.<sup>12</sup>

Each step of this process—deposition of the initiator monolayer, pattern generation in this layer via radiation exposure, and amplification of the pattern via polymerization—impacts the process timing and fidelity of the final pattern grown. This article discusses the characterization of the initiator monolayer reactivity during patterning and its impact on the patterning process time and fidelity.

## II. EXPERIMENT

### A. Initiators

Two initiators were synthesized and analyzed in this study, and their general structures are shown in Fig. 2.<sup>13</sup> The

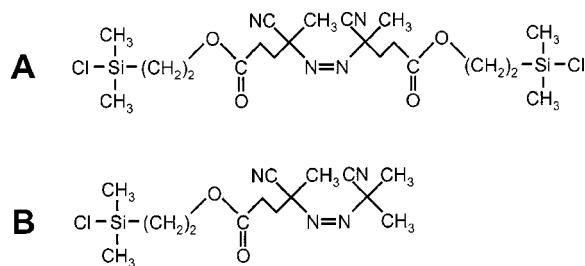


FIG. 2. Structure of the two surface bound azo radical initiators used in this work.

synthesis of the two initiators was performed using protocols reported previously.<sup>14,15</sup> Both of these initiators have chlorosilane anchoring groups for attaching the initiator to the hydroxyl terminated surfaces of metals and oxides, and they contain reactive azo groups which can form radicals when exposed to either heat or ultraviolet light. The difference between the two materials lies in the end group. Initiator A is symmetric, and thus it possesses a long carbon tail and chlorosilane anchoring end group on both ends of the molecule. In contrast, Initiator B only possesses one chlorosilane anchoring end group and is simply methyl terminated on the opposite end of the molecule.

### B. Preparation of initiator coated silicon samples

Silicon sample surfaces were initially cleaned using an RCA cleaning method. Each silicon sample was first placed in an SC-1 bath (consisting of water, hydrogen peroxide, and ammonia mixed in a volume ratio of 5:1:1, respectively) for 10 min at 60 °C. Each sample was then placed in a hydrofluoric acid (HF) bath (a 50:1 volume mixture of HF and water) for 15 s at 25 °C. Each sample was finally placed in an SC-2 bath (consisting of water, hydrogen peroxide, and hydrochloric acid mixed in a 5:1:1 volume ratio) for 10 min at 60 °C. This procedure cleans the surface of the silicon sample and removes the original silicon native oxide, replacing it with a clean silicon oxide surface. After each of these process steps, the sample was rinsed with deionized (DI) water for 10 min. Each sample was then placed in a 1 molar nitric acid (1 M HNO<sub>3</sub>) solution for 2 h, removed from the solution, and dried under nitrogen. Previous studies have shown that use of the nitric acid bath can increase the hydroxyl content of the clean silicon surface.<sup>15</sup> Initiator was deposited onto the clean silicon substrates by placing each sample in a 5 mM solution of the appropriate initiator in toluene for approximately 24 h. The initiator solutions were maintained under an argon atmosphere.

### C. X-ray photoelectron spectroscopy data calibration and analysis

The rates of decomposition of the surface bound initiators were monitored using a Physical Electronics (PHI) x-ray photoelectron spectroscopy (XPS) system. This was accomplished by using the XPS to determine the relative surface concentration of an active initiator as a function of ultraviolet

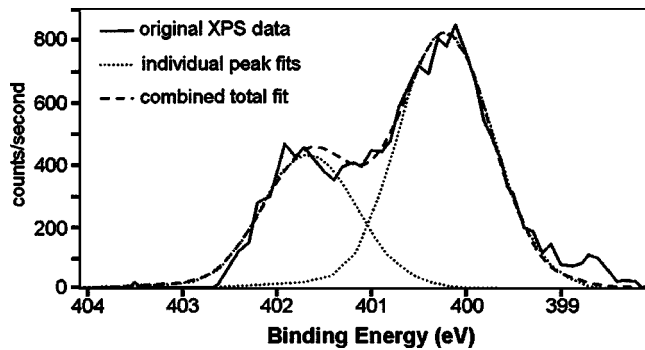


FIG. 3. Nitrogen XPS spectrum for unexposed initiator A monolayer.

exposure dose. Monochromatic Al  $K\alpha$  x rays at 1486.6 eV were used to excite this monolayer system. X rays that impinge upon the sample from the XPS can also decompose the initiator. Therefore, before analyzing the relative surface concentrations of the initiator using the XPS, a calibration curve was established to determine the extent to which the x rays decompose the monolayer. A silicon sample coated with the initiator was placed in the XPS and data scans were collected at various time intervals while the x-ray source exposed the surface.

### 1. Determining the location of the azo peak in XPS data

The first task in evaluating these data was to determine the location of the azo (N=N) peak. There are two types of nitrogen in the system. The first stems from the nitrogen triply bound to carbon in the cyano (C≡N) groups in the initiator molecule. The second stems from the azo group. A scan of the nitrogen region of the XPS data for initiator A is shown in Fig. 3. The largest peak in the spectrum is centered at 400.2 eV and was assigned to the nitrogen in the cyano group. This assignment was made based on literature values;<sup>16,17</sup> therefore, the second peak at 401.7 eV was assigned to the azo nitrogen. In these initial scans, the full width at half maximum of both peaks was equal and assigned to 1.15 eV. For all subsequent fitting, the peaks were assumed to be Gaussian and the full width at half maximum of both of the peaks was assumed to be equal.

### 2. Normalization of XPS data

The area under the azo (N=N) peak in the XPS spectrum was normalized to the area of the SiO peak (at 103.3 eV) to determine the relative concentration of the active initiator on the surface of a given sample. The electrons reaching the XPS detector were emitted from the top 50 Å of the film which consisted of ~20 Å of the initiator layer, the ~20 Å of native silicon dioxide, and ~10 Å of the underlying silicon substrate. The thickness of the monolayer decreased as it decomposed, and thus a greater contribution of the electrons reaching the detector could be emitted from the silicon substrate. However, in the stack that was analyzed, the entire native silicon oxide layer was sampled in all XPS studies and its thickness remained constant. A constant number of elec-

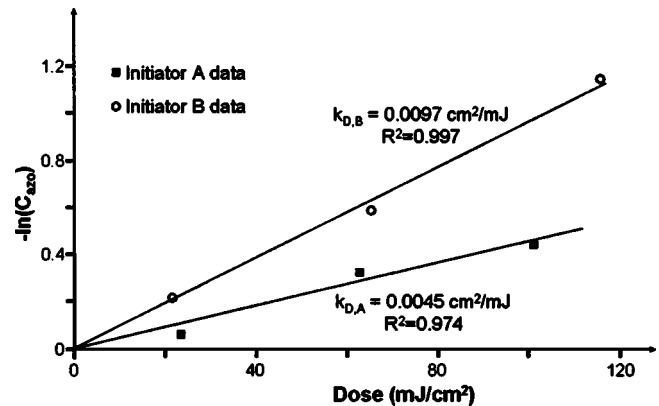


FIG. 4. Plot of the negative natural logarithm of the normalized surface azo initiator concentration as a function of exposure dose. The linearity of the data confirms first order decomposition kinetics and appropriate photodecomposition rate constants are shown for both initiators.

trons were therefore emitted from the silicon oxide layer. The signal from this layer could thus be used as a reference for normalization of the surface species concentrations.

After identifying the azo peak and the SiO peak to which it should be normalized, a calibration curve for the decomposition of the initiator upon exposure to x rays was created. A plot of the natural logarithm of the azo peak area versus x-ray exposure time to the x rays from the XPS system was generated. This plot exhibited a linear relationship; therefore, the decomposition of the monolayer due to x-ray exposure in the XPS is a first order process. This calibration plot was used to adjust all XPS measurements of the azo peak area to account for the varying lengths of time that samples were exposed to the x-ray beam during XPS analysis. Most of the XPS spectra were acquired in less than 2 min; therefore, less than 20% of the initiator decomposed as a result of data collection.

## III. RESULTS AND DISCUSSION

### A. Photochemical decomposition

The normalized azo concentration as a function of DUV (248 nm) exposure dose for initiators A and B was computed from the XPS data generated. The decomposition of both initiators followed first order kinetics as indicated by Fig. 4 which shows a linear relationship between the natural logarithm of the fraction of initiator remaining on the surface as a function of dose. The rate constants, which can be found from the slope of the lines in Fig. 4, are  $4.5 \times 10^{-3} \text{ cm}^2/\text{mJ}$  for initiator A and  $9.7 \times 10^{-3} \text{ cm}^2/\text{mJ}$  for initiator B. Using these rate constants, one can derive a simple expression to estimate the dose required ( $D$ ) to achieve a desired fraction of initiator remaining ( $X$ ) on the surface. This expression is shown in Eq. (1) below,

$$D = -\frac{\ln(x)}{k_{D,i}} \quad (1)$$

Using this equation, one finds that to achieve 99% conversion of initiator A by exposure to DUV light one must

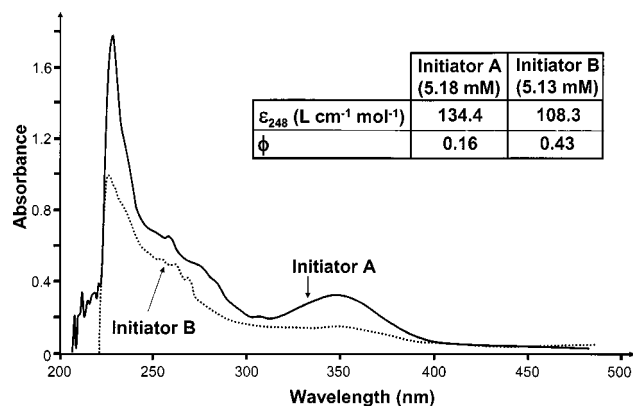


FIG. 5. Ultraviolet absorption spectra of initiators A and B. The spectra were obtained in methylene chloride ( $CH_2Cl_2$ ). The table shows the molar absorptivity and quantum efficiency for each initiator based on calculations using the absorption data and photodecomposition rate constants.

provide an exposure dose of approximately  $1\ J/cm^2$ . However, the dose required to decompose 99% of initiator B is only  $475\ mJ/cm^2$ . These doses are lower than those observed by other groups who have also been working on patterning schemes based on the decomposition of self-assembled monolayers on flat surfaces. Ultraviolet doses between  $1$  and  $20\ J/cm^2$  are usually required to fully decompose straight chain hydrocarbon SAMs to form patterns on surfaces.<sup>18–21</sup> In one case, a dose of  $54\ J/cm^2$  was required to pattern the SAM.<sup>22</sup> There are only two reports in the literature of SAMs having a greater sensitivity than this. Researchers at the Naval Research Laboratory have been able to decompose phenyl terminated SAMs and amine terminated SAMs at doses of  $\sim 400\ mJ/cm^2$  by exposing a wavelength of  $193\ nm$ .<sup>23,24</sup> At this wavelength, most organic compounds have strong absorbance. Therefore, many compounds show strong ablation phenomena when exposed to  $193\ nm$  radiation. It would be anticipated that the compounds studied in this work would also show higher reaction rates when using  $193\ nm$  light instead of the  $248\ nm$  exposures used here.

Though the doses required to decompose these samples are lower than those reported by others, they are unacceptable for a conventional sub- $100\ nm$  semiconductor lithography application. The International Technology Roadmap for Semiconductors (ITRS) states that the sensitivities of current and future generation resists should be on the order of  $10\ mJ/cm^2$ ;<sup>25</sup> therefore, for the SMIP approach to be useful in such applications the sensitivity of the SMIP initiators must be improved significantly. A comparison of the results between initiators A and B provides insight into future initiator design. Initiator B decomposes at twice the rate of initiator A. These rate constants are a product of the molar absorptivity ( $\epsilon$  [ $cm^2/mJ$ ]) and the quantum efficiency ( $\Phi$  [dimensionless]) of the molecules as shown in Eq. (2),

$$k = \epsilon \phi. \quad (2)$$

Collecting ultraviolet spectra of the molecules aids in elucidating which factor is predominant in the differences observed in their photochemical behavior. Figure 5 shows the

solution ultraviolet spectra of these materials. The table above the spectra shows the molar absorptivity and the calculated quantum efficiency of these molecules at  $248\ nm$ . Initiator A exhibits a molar absorptivity that is 30% higher than that of initiator B at this wavelength. However, the rate constant of photochemical decomposition of initiator B is twice that of initiator A. This implies that the difference in the rate constants is primarily due to differences in the quantum efficiency of each molecule.

Consideration of the structure of these two initiators can give insight as to why the quantum efficiency of initiator B is almost three times larger than that of initiator A. Both ends of initiator A have the ability to bind to the surface. If both ends of initiator A are tethered to the surface, one might expect the probability of recombination of the fragments of this molecule to be large. Even if only one end group of initiator A is tethered to the surface, the other end is bulky and thus possesses a lower mobility and volatility than the photochemical fragment produced by photochemical cleavage of initiator B. Thus, this initiator A fragment then would not be able to dissociate and leave the surface as easily after the molecule has been photochemically cleaved. The large fragment of the initiator A molecule will most likely recombine with the other radical fragment on the surface. Initiator B is only singly bound to the surface. As this initiator decomposes, the small nontethered fragment of the initiator can leave the surface easily and the probability of recombination is minimized.

## B. Impact of photochemical initiator decomposition on patterning

After the initiator is patterned in this positive tone SMIP process, the entire substrate is polymerized either thermally or photochemically. For a positive tone process, it would be desired that only the unexposed areas of the initiator participate in this final polymerization. However, since there is essentially never a situation in which all of the initiator molecules in the exposed region are decomposed, it is important to understand the tradeoffs between exposure dose and the resulting polymer defect density and sizes in the exposed regions. The information presented above can be used to make a rough prediction of the polymer features formed in the exposed regions using a positive tone process. This reduced concentration of active initiators must not generate polymer that will essentially “blur out” the latent chemical monolayer pattern during the polymerization. Therefore, one criterion that can be used for signaling when the pattern is lost is when the spacing between two chains is equal to or smaller than the dimensions of the polymers grown. Estimating the graft density of initiator ( $\Gamma$ ) to be on the order of  $10^{14}$  molecules per square centimeter,<sup>26</sup> assuming a radical efficiency ( $f$ ) of  $0.35$ ,<sup>9</sup> and using the data presented above, calculating the spacing between two polymer chains in the exposed region of the films is straightforward. The percentage of photochemically decomposed material can be calculated from the rate constant of photochemical decomposition ( $k_{D,i}$ ) and the dose applied ( $D$ ). This level of decomposition di-

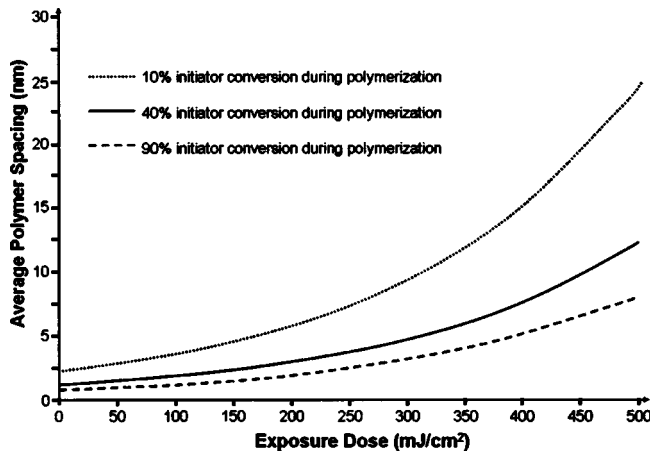


FIG. 6. Plot of the average center-to-center polymer chain spacing in an exposed initiator B monolayer as a function of 248 nm exposure dose to the monolayer. Several curves for different initiator polymerization conversions are shown.

rectly affects the initial graft density of active initiator sites on the exposed surface before polymerization. Using this information, the average spacing between polymer chains in the exposed “deactivated region” as a function of the polymerization conversion ( $x_p$ ) can be calculated via Eq. (3). If the spacing of the polymer chains at a particular polymerization conversion is significantly greater than the expected radius of gyration of the polymers grown at that conversion, then the dose used to photochemically decompose the initiator layer should be sufficient to result in at least some pattern formation,

$$d = \sqrt{\frac{1}{\exp(-k_{D,i}D)\Gamma f x_p}}. \quad (3)$$

Figure 6 displays the average spacing between polymer chains grown in the exposed “deactivated” (photochemically decomposed) regions of the film (as a result of the thermal polymerization after growth of a polymer film) versus exposure dose using 248 nm (DUV) light at 40% polymerization conversion for the more sensitive initiator B. It was previously shown that a polymerization conversion of at least 40% was typically needed to create films from unexposed initiator layers which possessed reasonable uniformity and whose thickness could be measured via ellipsometry.<sup>15</sup> At this 40% polymerization conversion, an exposure dose of at least 450 mJ/cm<sup>2</sup> is needed for initiator B to separate the polymer chains in the “deactivated” region of the monolayer by tens of nanometers. If a polymer with a radius of gyration greater than the separation of these polymer chains is grown, the pattern will essentially fill in to form a continuous film. Since the radius of gyration of the polymers typically grown on surfaces using these radical polymerization methods is on the order of tens of nanometers,<sup>22</sup> it can be concluded that a dose of at least 450 mJ/cm<sup>2</sup> would be required in order to even achieve some level of pattern definition for positive tone imaging using initiator B. A similar exercise for initiator A shows that an exposure dose of at least 1000 mJ/cm<sup>2</sup>

would be required. These exposure doses translate into a requirement of approximately 99% photochemical initiator decomposition in order to achieve some level of pattern definition.

#### IV. SUMMARY AND CONCLUSIONS

The rates of decomposition at deep UV wavelengths (248 nm) of two self-assembled azo compounds on silicon native oxide surfaces have been examined via x-ray photoelectron spectroscopy (XPS). At this wavelength, these molecules decompose via first order processes with rate constants of  $4.5 \times 10^{-3}$  cm<sup>2</sup>/mJ and  $9.7 \times 10^{-3}$  cm<sup>2</sup>/mJ. These rates of decomposition are faster than those reported in the literature for patterning other monolayer systems. The difference in reactivity of these two azo molecules is predominantly due to differences in their quantum efficiency, which in this case is believed to be largely controlled by the size of the nontethered radical fragment generated from the initiator. For the positive tone SMIP process reported in this work, it was found that approximately 99% decomposition of the initiator monolayer was needed in order to create high resolution polymer patterns. Using the measured photoreaction rate constants, doses of approximately 1 J/cm<sup>2</sup> and 400 mJ/cm<sup>2</sup> are needed to achieve 99% decomposition of the initiator monolayers used in this work. Thus, even though these monolayers are very sensitive compared to many other monolayer patterning systems studied previously, the high doses required for successful positive tone patterning make a positive tone process using these initiators undesirable for low wavelength lithography applications in microelectronics manufacturing.

<sup>1</sup>S. Okazaki, *Future of Optical Lithography*, in 18th Congress of the International Commission for Optics: Optics for the Next Millennium (SPIE-The International Society for Optical Engineering, San Francisco, CA, 1999), p. 329.

<sup>2</sup>T. M. Bloomstein, M. Rothschild, R. R. Kunz, D. E. Hardy, R. B. Goodman, and S. T. Palmacci, *J. Vac. Sci. Technol. B* **16**, 3154 (1998).

<sup>3</sup>A. C. Cefelas, E. Sarantopoulou, E. Gogolides, and P. Argitis, *Microelectron. Eng.* **53**, 123 (2000).

<sup>4</sup>R. J. Hung, H. V. Tran, B. C. Trinque, T. Chiba, S. Yamada, D. P. Sanders, E. F. Connor, R. H. Grubbs, J. Klopp, J. M. J. Frechet, B. H. Thomas, G. J. Shafer, D. D. DesMarteau, W. Conley, and C. G. Willson, *Proc. SPIE* **4345**, 385 (2001).

<sup>5</sup>S. V. Postnikov, M. H. Sovervell, C. L. Henderson, S. Katz, C. G. Willson, J. Byers, A. Qin, and Q. Lin, *Proc. SPIE* **3333**, 997 (1998).

<sup>6</sup>S. Mori, T. Morisawa, N. Matsuzawa, Y. Kaimoto, M. Endo, T. Matsuo, K. Kuhara, and M. Sasago, *Jpn. J. Appl. Phys., Part 1* **37**, 6734 (1998).

<sup>7</sup>S. Mori, T. Morisawa, N. Matsuzawa, Y. Kaimoto, M. Endo, T. Matsuo, K. Kuhara, and M. Sasago, *J. Vac. Sci. Technol. B* **16**, 3739 (1998).

<sup>8</sup>O. Prucker and J. Ruehe, *Langmuir* **14**, 6893 (1998).

<sup>9</sup>O. Prucker and J. Ruehe, *Macromolecules* **31**, 592 (1998).

<sup>10</sup>C. Willson, A. Hult, and S. A. MacDonald, *Polym. Mater. Sci. Eng.* **52**, 339 (1985).

<sup>11</sup>H. F. Johnson, A. T. Jamieson, S. N. Ozair, T. Farmer, Z. Hogan, S. MacDonald, and C. G. Willson, *AICHE National Meeting*, San Francisco, CA, 2003.

<sup>12</sup>X. H. Chen, L. M. Tolbert, D. W. Hess, and C. L. Henderson, *Macromolecules* **34**, 4104 (2001).

<sup>13</sup>X. H. Chen, L. M. Tolbert, C. L. Henderson, D. W. Hess, and J. Ruehe, *J. Vac. Sci. Technol. B* **19**, 2013 (2001).

<sup>14</sup>X. H. Chen, Ph.D. dissertation, Georgia Tech., 2000.

<sup>15</sup>K. M. McCoy, Ph.D. dissertation, Georgia Tech., 2004.

<sup>16</sup>D. R. Jung, D. E. King, and A. W. Czanderna, *J. Vac. Sci. Technol. A* **11**,

- 2382 (1993).
- <sup>17</sup>F. Tao, W. S. Sim, G. Q. Xu, and M. H. Qiao, *J. Am. Chem. Soc.* **123**, 9397 (2001).
- <sup>18</sup>H. Sugimura, *J. Vac. Sci. Technol. A* **19**, 1261 (2001).
- <sup>19</sup>L. Hong, H. Sugimura, T. Furukawa, and O. Takai, *Langmuir* **19**, 1966 (2003).
- <sup>20</sup>N. Saito, K. Hayashi, H. Sugimura, and Osamu Taka, *J. Mater. Chem.* **12**, 2684 (2002).
- <sup>21</sup>H. Sugimura, T. Hanji, O. Takai, K. Fukuda, and H. Misawa, *Mater. Res. Soc. Symp. Proc.* **584**, 163 (2000).
- <sup>22</sup>D. A. Tryk, X. Yang, K. Hashimoto, and A. Fujishima, *Bull. Chem. Soc. Jpn.* **71**, 31 (1998).
- <sup>23</sup>C. S. Dulcey, J. H. Georger, V. Krauthamer, D. A. Stenger, T. L. Fare, and J. M. Calvert, *Science* **252**, 551 (1991).
- <sup>24</sup>W. J. Dressick, C. S. Dulcey, M.-S. Chen, and J. M. Calvert, *Thin Solid Films* **284-285**, 568 (1996).
- <sup>25</sup>International Roadmap for Semiconductors, 2002 Update, 63 (2002).
- <sup>26</sup>Z. Zekkat, J. Wood, Y. Geerts, and W. Knoll, *Langmuir* **12**, 2976 (1996).